PERGAMON

Journal of Structural Geology 21 (1999) 1027–1038

JOURNAL OF STRUCTURAL GEOLOGY

www.elsevier.nl/locate/jstrugeo

Normal fault corrugation: implications for growth and seismicity of active normal faults

David A. Ferrill*, John A. Stamatakos, Darrell Sims

Center for Nuclear Waste Regulatory Analyses, Southwest Research Institute, 6220 Culebra Road, San Antonio, TX 78238, USA

Received 3 February 1998; accepted 30 September 1998

Abstract

Large normal faults are corrugated. Corrugations appear to form from overlapping or en échelon fault arrays by two breakthrough mechanisms: lateral propagation of curved fault-tips and linkage by connecting faults. Both mechanisms include localized fault-parallel extension and eventual abandonment of relay ramps. These breakthrough mechanisms produce distinctive hanging wall and footwall geometries indicative of fault system evolution. From such geometries, we can estimate the positions of tilted relay ramps or ramp segments and ramp internal deformation in incompletely exposed or poorly imaged fault systems. We examine the evolution of normal fault corrugations at Fish Slough (California), Yucca Mountain (Nevada), and Pleasant Valley (Nevada), in the Basin and Range province. We discuss how evolution of the Pleasant Valley and Yucca Mountain systems relates to seismicity. For example, the 1915 Pleasant Valley earthquake produced four en échelon ruptures that appeared as overlapping segments of a single immature fault at depth. At Yucca Mountain, we argue that an en échelon array, which includes the Solitario Canyon and Iron Ridge faults, should be considered a single source, such that western Yucca Mountain could experience up to a M_w 6.9 earthquake compared to M_w 6.6 estimates for the largest individual segment.

1. Introduction

Many large normal faults are corrugated, having ridges and grooves that plunge down the dip of the fault surface parallel or subparallel to slip. Small-scale corrugations form over several orders of magnitude in size up to meters in wavelength (Hancock and Barka, 1987). Large-scale corrugations (with wavelengths of hundreds of meters to kilometers) are common and are expressed at the ground surface as a curved or angular undulation of the fault trace (Donath, 1962; Ramsay and Huber, 1987; Machette et al., 1991; Holm et al., 1994; Peacock and Sanderson, 1994; Childs et al., 1995; Morley, 1995; Platt, 1995; Ferrill et al., 1996a). Large-scale corrugations of normal faults form by various mechanisms including reactivation of preexisting faults or fractures (e.g. Donath, 1962), folding of fault surfaces (e.g. Holm et al., 1994), and progressive breakthrough of originally segmented (e.g. en échelon) fault systems. The details of corrugation patterns provide us with important kinematic indicators of normal fault evolution, particularly in terms of how en échelon faults and their connecting structures interact to develop large fault systems.

Examination of natural normal fault systems from the Basin and Range province of the western United States reveals that large normal faults generally grow by intersection and capture of overlapping en échelon faults rather than by lateral propagation of a single rupture surface at fault-tips (Anders and Schlische, 1994; Schlische and Anders, 1996). Fault growth occurs by intersection (or linkage) and amalgamation of overlapping fault segments either by lateral (curved) propagation of the en échelon fault-tips or formation of new connecting faults (Peacock and Sanderson, 1994; Childs et al., 1995).

These fault growth mechanisms produce distinctive hanging wall and footwall geometries that reveal infor-

* Corresponding author.
E-mail address: dferrill@swri.edu (D.A. Ferrill)

0191-8141/99/$ - see front matter
PII: S0191-8141(99)00017-6

mation about the mechanism of fault growth. In this paper, we present three examples of normal fault systems from the Basin and Range province of the western United States to illustrate normal fault growth mechanisms. Based on these observations, we propose a generalized model for normal fault development by capture that produces corrugated fault surfaces. Fault corrugation geometry is indicative of specific hanging wall and footwall structures, which can reveal important clues about the potential for fluid (hydrocarbon or groundwater) traps or baffles to form or compartmentalize oil and gas fields and aquifers. Furthermore, secondary deformation related to normal fault growth is important to natural fracturing and faulting of reservoirs and seals, or aquifers and aquitards. Understanding the detailed geometry and evolution of normal faults is also important to assessments of earthquake and ground rupture hazards. Recognition of linked normal fault systems in the early stages of development may be the key to avoiding underestimation of seismic hazard in extensional terranes.

2. Normal fault corrugations from en échelon arrays

En échelon arrangement of normal-fault offsets indicates either a system of unconnected overlapping (en échelon) faults or en échelon branching of a single fault (Fig. 1; Childs et al., 1995; Willemse et al., 1996; Willemse, 1997). En échelon extension fractures and faults have traditionally been considered the product of simple shear parallel to the enveloping surfaces of the fracture system (e.g. Sylvester, 1988; An and Sammis, 1996). Recent detailed investigations, however, indicate that en échelon arrangement of normal faults or fault segments is common in extensional settings, and not simply restricted to strike-slip deformation (e.g. figs. 4-34 and 4-35 in Lowell, 1985; Anders and Schlische, 1994; Childs et al., 1995; Dawers and Anders, 1995; Willemse, 1997). Regardless of the mechanical origin of en échelon fault systems or en échelon branching faults (Fig. 1a), we envision two mechanisms by which increasing displacement eventually produces breakthrough of the system and fault corrugation: (1) lateral curved propagation and linkage of faults (Fig. 1b); or (2) formation of new connecting faults that breach the relay ramps (Fig. 1c; Peacock and Sanderson, 1994; Trudgill and Cartwright, 1994).

2.1. Mechanism I—lateral propagation of curved fault-tips

Corrugated fault formation is divided into three stages. First, en échelon fault-tips propagate laterally to overlap. Subsequently, increasing displacement gradients on overlapping faults produce vertical- or steeply inclined-axis rotations (a function of heave gradient), and ramp tilting (a function of throw gradient; Fig. 1b; Peacock and Sanderson, 1991, 1994; Trudgill and Cartwright, 1994). Extension parallel to fault strike is common in relay ramps. This strike-parallel extension accommodates displacement gradients (manifest by tilting produced by throw gradients, and vertical-axis rotation produced by heave gradients) and can lead to breaching of relay ramps (Fig. 1a). Local ramp extension commonly combines with regional extension (concentrated in the relay ramp because of increasing displacement gradient in overlap zone) to produce oblique structures that accommodate both local and regional strain.

In the third stage, fault-tips propagate along curved paths to intersect the next en échelon fault, resulting in a scallop-shaped corrugated fault surface, with cuspate ridges that correspond to fault segment intersections (Fig. 1b). In isotropic rocks, curved propagation is

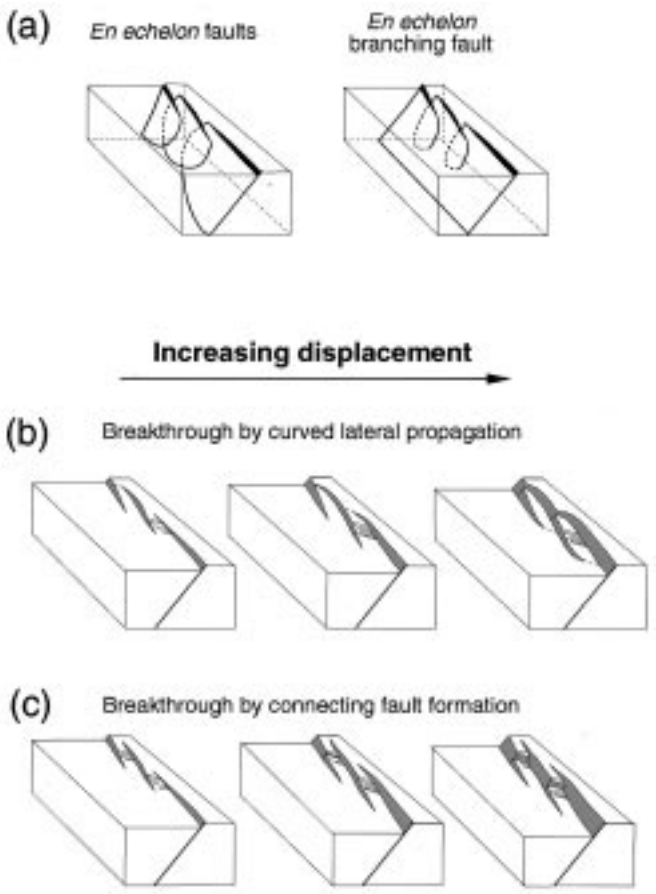

Fig. 1. Block diagrams illustrating (a) topology of en échelon fault systems and en échelon branching faults, (b) sequence of evolution of en échelon normal fault array or en échelon branching normal fault involving linkage and breakthrough by lateral propagation of curved fault-tips, and (c) sequence of evolution of en échelon normal fault array or en échelon branching fault system involving linkage and breakthrough by connecting fault formation.

commonly produced by the influence of a nearby fault on the local fault-tip stress field during fault propagation. Breakthrough along the upthrown or downthrown fault block leaves relict fault-tips and relay ramps attached to the hanging wall or footwall, respectively. Breakthrough along both upthrown and downthrown traces produces fault bounded blocks (horses) between two corrugated surfaces, forming an anastomosing fault zone.

2.2. Mechanism II—linkage by connecting faults

Stages (1) and (2) of corrugated fault formation by connecting fault formation (Fig. 1c) are identical to the first stages in mechanism I. In stage (3), increasing displacement gradient in the overlap causes relay ramp tilting and extension to increase and results in the formation of connecting faults that link displacement on overlapping faults. This occurs where fault throw increases disproportionately to fault-tip propagation. If lateral fault propagation continues proportionally with increasing throw, then the ramp may lengthen without steepening. This process of fault (and ramp) lengthening, rather than ramp steepening, occurs without intensifying local extension in the ramp that leads to breakthrough. Linkage by connecting faults leaves relict fault-tips and relay ramp segments attached to both hanging wall and footwall.

3. Examples from the Basin and Range, USA

3.1. Fish Slough fault system, Volcanic Tableland, Owens Valley (California)

The Volcanic Tableland in northern Owens Valley, California (Fig. 2) is capped by the 738 ± 3 ka Bishop Tuff (Izett et al., 1988), deposited on air fall ash, and fluvially reworked Quaternary volcaniclastic deposits and other sedimentary basin fill (Bateman, 1965). After deposition, the region was extended. Numerous north–south-trending normal faults and fault segments with fault spacings of about 1–2 km resulted. Growth across some faults indicates that faulting was active prior to tuff deposition (Bateman, 1965).

Because of this geologic setting, the ~150 m thick capping volcanic tuff represents a time-stratigraphic marker. Topography of the capping horizon records post-738 ka faulting (Fig. 2; e.g. Bateman, 1965). Because of their excellent exposure, Bishop Tuff fault scarps have provided much of the landmark data in the development of fault scaling relationships (Dawers et al., 1993; Scholz et al., 1993; Dawers and Anders, 1995; Willemse et al., 1996; Willemse, 1997).

The southern part of the Volcanic Tableland is essentially a gentle southeast-dipping homocline with an eastward rollover into the Fish Slough fault system (Fig. 2). The rollover continues eastward to the White Mountains fault. The crest of the rollover is broken by a northwest-trending crestal graben system defined on the west by an eastward-convex segmented normal fault system (studied by Dawers and Anders, 1995) and on the east by a northwest-trending en échelon fault array (Fig. 2). Throughout the Volcanic Tableland, faults or fault segments generally trend north–south and show normal offsets (Fig. 2). North of UTM 4146000, the fault scarps are arranged into six dominant northwest-trending en échelon fault systems, three dipping west and three dipping east. South of UTM 4146000, the en échelon arrangement of faults is not so evident and fault segmentation with both right and left stepping arrangements is present.

Although suggestive of strike-slip deformation, the fault pattern in the Volcanic Tableland appears to be largely a dip-slip phenomenon. Ancient stream channels that predate normal faulting have been offset up and down across the normal fault scarps without significant strike-slip offset (Bateman, 1965; Dawers et al., 1993). One stream channel that extends for a distance of 7 km in the southern part of the Volcanic Tableland (Bateman, 1965) has been offset vertically across at least six faults with virtually no discernible horizontal displacement. Another paleostream channel, cut by the en échelon segmented fault system that bounds the west side of the crestal graben, shows only dip-slip offset across three fault scarps with no lateral displacement (Dawers et al., 1993).

The largest-displacement fault cutting the capping tuff in the Volcanic Tableland is the >15 km long Fish Slough fault system, a north–south-trending fault system with nearly 150 m throw that defines the eastern edge of the Fish Slough drainage valley. This fault system can be subdivided into three primary sections (Fig. 2a). The southern section, which is strongly corrugated near its southern end, overlaps in a left-stepping arrangement and is separated from the central section by a southeast-tilted relay ramp. Associated with the corrugations are two south-dipping wedge shaped fault blocks, exposed on the footwall fault surface (Fig. 2a and c). The two wedge-shaped fault blocks are defined on their west sides by (relict?) fault-tips. Throw gradients produced dips of 10–15° in both fault blocks (Fig. 2d and e). The southern fault block contains several small-displacement normal faults (both east and west dipping) oblique to the block bounding faults (see three scarps within tilted fault block shown in Fig. 2d).

In terms of our model for fault growth, the southern section of the Fish Slough fault system represents a fairly mature stage of fault growth indicated by: (1) complete breakthrough of the footwall fault surface by lateral fault-tip propagation along curved trajectories

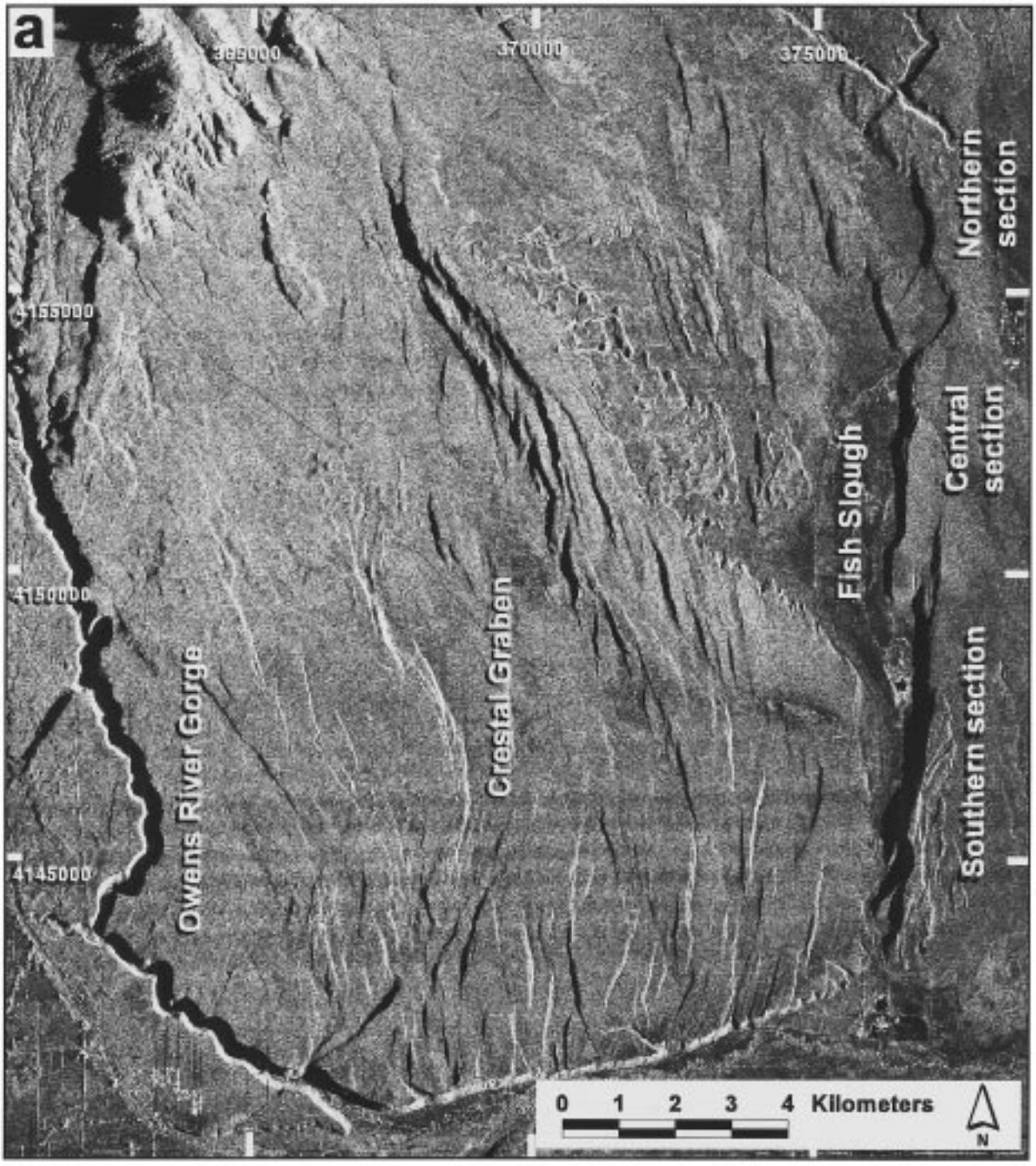

Fig. 2. Faulting in the Volcanic Tableland north of Bishop, California. (a) Side looking airborne radar (illumination from east) illustrates east-dipping fault scarps (brightly illuminated) and west-facing scarps (in shadow). (b) Three-dimensional model of the Volcanic Tableland (VE = 5×) illustrates crestal graben and rollover into the Fish Slough fault system. (c) Oblique aerial photograph looking northwest across the southeastern corner of the Volcanic Tableland from Bateman (1965) (photo by Roland Von Huene from Bateman, 1965) shows corrugated shape of the Fish Slough fault. (d) Field photograph looking east at the southern tilted fault block (relict relay ramp) along the southern segment of the Fish Slough fault system shows small faults within the block. (e) Distance–displacement (throw) diagram for Fish Slough fault system. Individual fault segments are represented by thin solid lines and cumulative throw is represented by a dashed line.

(Fig. 2a and c); (2) oblique normal faults in the southern relay ramp indicating ramp extension (Fig. 2d); and (3) relict en échelon fault segments and relay ramps attached to the hanging wall block (Fig. 2a, c and d). In contrast, the relay ramp between the southern and central sections of the Fish Slough fault system remains intact (Fig. 2a and c). Lack of break-through by connecting faults or lateral propagation of

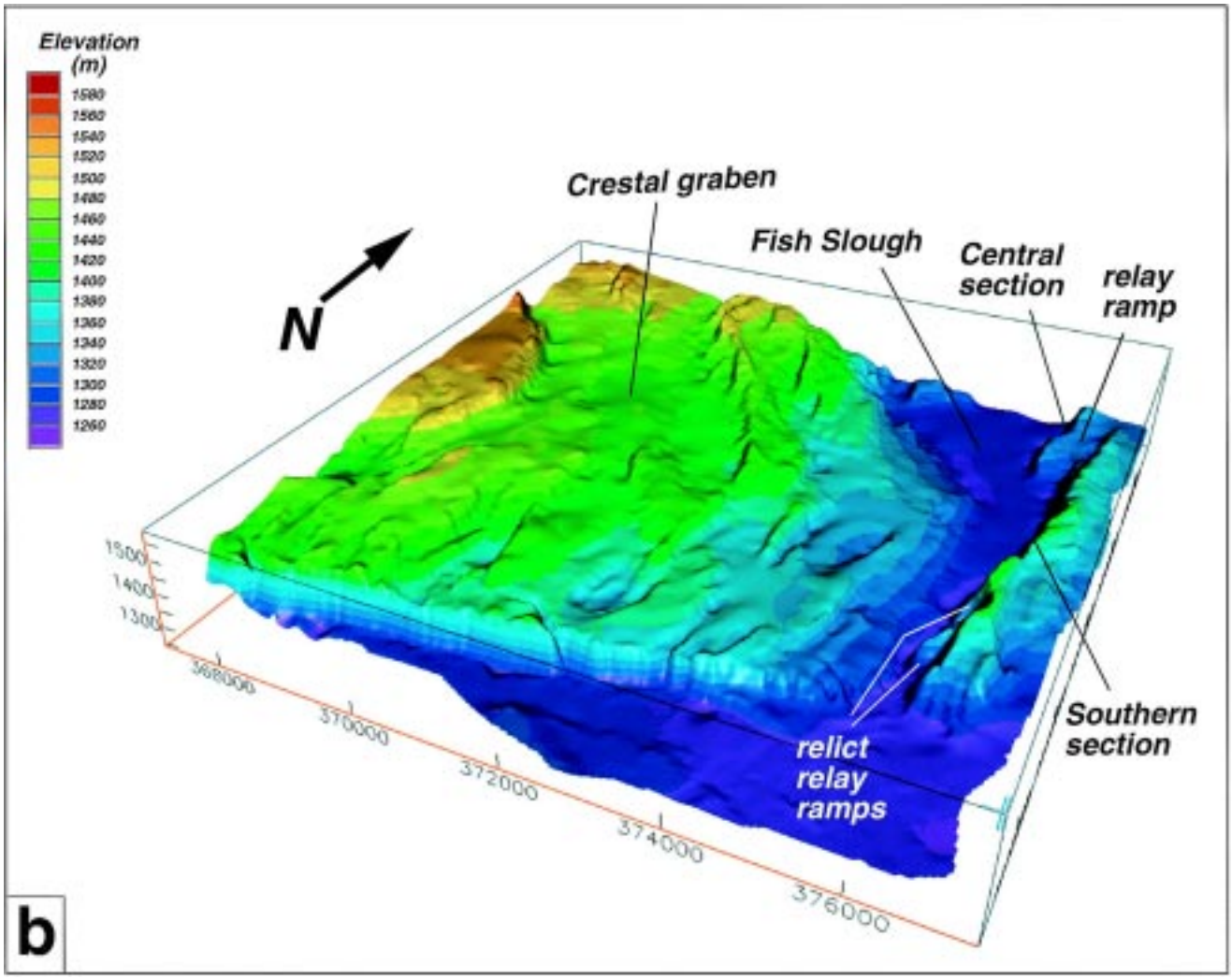

Fig. 2. (*continued*)

curved fault-tips is probably due to the smaller displacement gradients along the overlapping fault-tips and large offset (0.8 km) between overlapping fault-tips (Fig. 2a and e). The consistent regional east–west extension direction (Bellier and Zoback, 1995) and youth of the Fish Slough fault system (< 738 ka) suggest that in this case corrugations are produced by lateral curved propagation driven by the local fault-tip stresses rather than changes in the regional extension direction.

3.2. Solitario Canyon–Iron Ridge Fault System, Yucca Mountain (Nevada)

Yucca Mountain in southwestern Nevada, site of a proposed repository for high-level radioactive waste, is composed of a sequence of dominantly pyroclastic volcanic deposits that erupted from the Southwest Nevada Volcanic Field during the Miocene (e.g. Sawyer et al., 1994). These volcanic strata primarily dip gently eastward and have been cut by numerous faults. The west flank of Yucca Mountain is defined by a series of left stepping north–south-trending en échelon normal faults (Fig. 3). Southward increasing fault offsets coupled with greater fault block tilts indicate that displacement on the western Yucca Mountain fault system increases southward (Scott, 1990). This displacement gradient accommodates southward increasing rollover deformation in the hanging wall of the listric Bare Mountain Fault (Ferrill et al., 1996a,b).

Yucca Crest is a 19-km-long north–south-trending ridge bound along its western side by a fault line escarpment that follows the west-dipping Solitario Canyon, Iron Ridge, and Stagecoach Road faults (Fig. 3; Simonds et al., 1995; Day et al., 1998). These main west-dipping faults (and Yucca Crest) define a scalloped trend composed of linear north- (or north-north-

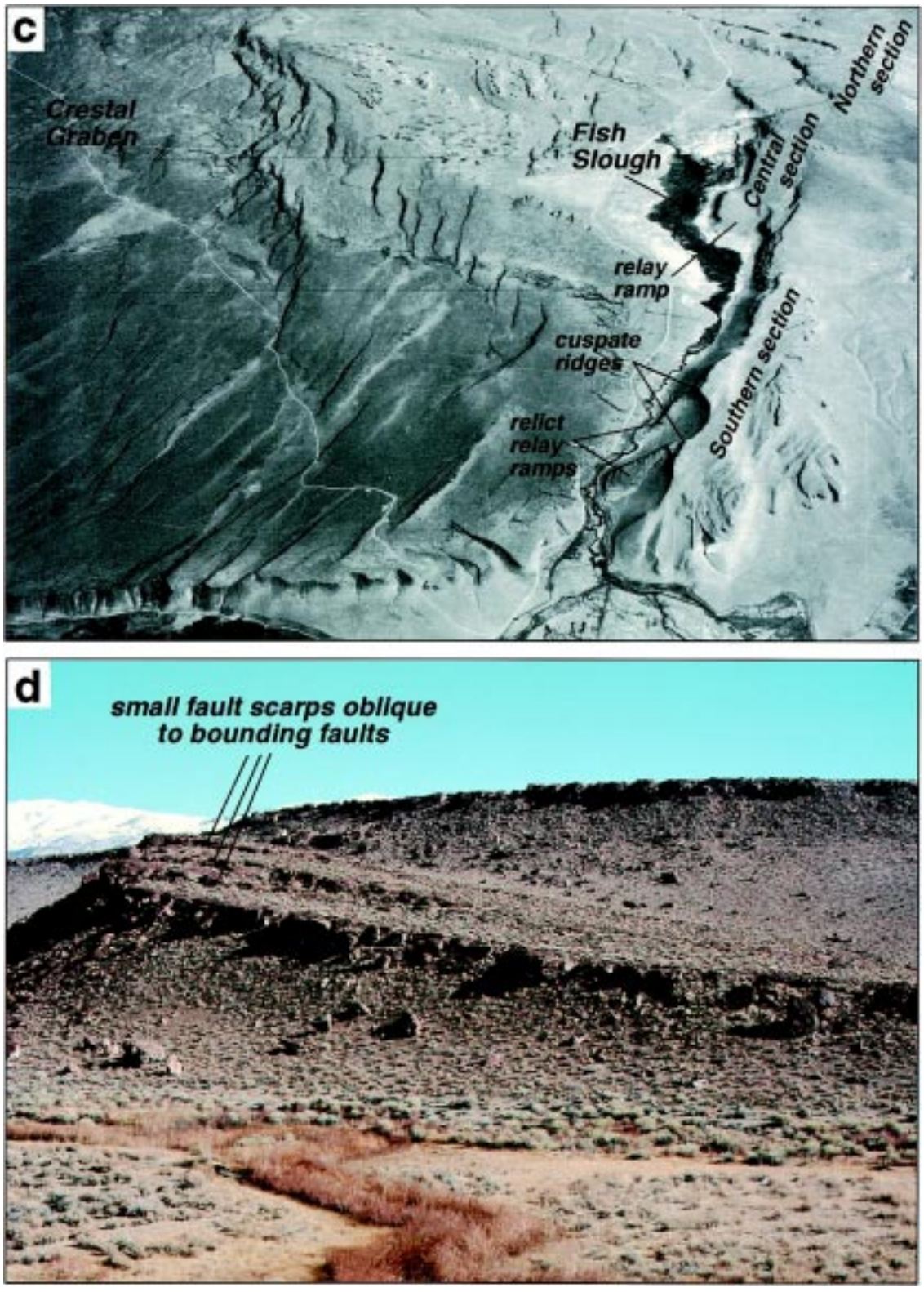

Fig. 2. (*continued*)

east-) trending segments, connected by discrete curvilinear northwest segments. For example, the north and south ends of the Iron Ridge fault (Fig. 3c) curve to trend northwestward, toward the Solitario Canyon and Stagecoach Road faults, respectively. Aside from the ends of the Iron Ridge fault, major northwest-trending

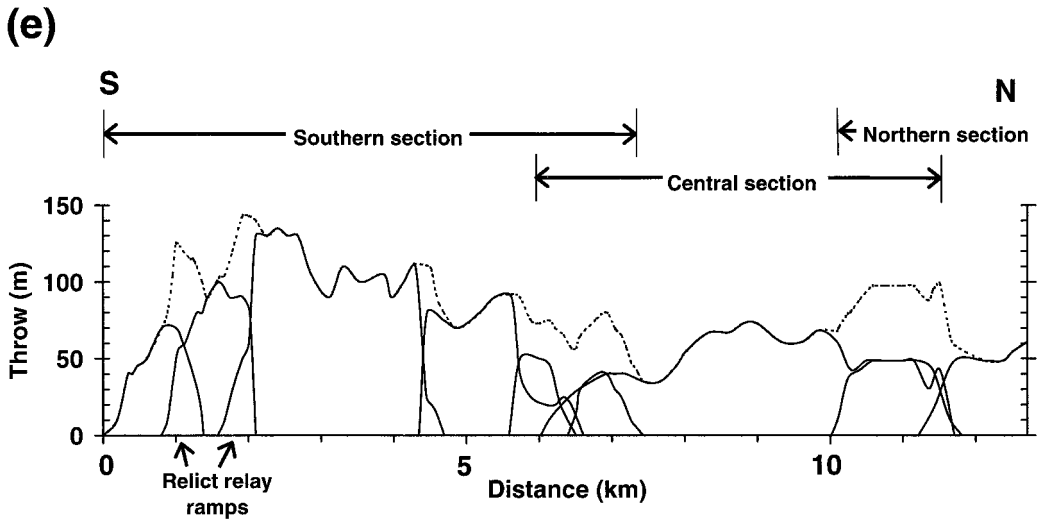

Fig. 2. (*continued*)

faults are not common in the western Yucca Mountain fault system. Fault blocks, however, are locally cut by small northwest-trending faults. One example is associated with the intersection of the Iron Ridge and Solitario Canyon faults. South of the intersection, these faults isolate a ridge of tuff in the footwall of the Solitario Canyon fault that, similar to the southernmost faulted relay ramp of the Fish Slough fault system, is obliquely cut by normal faults. The ridge is cut by at least 15 northwest-trending normal faults that parallel the northern end of the Iron Ridge fault where it curves northwestward into the Solitario Canyon fault (from map of Simonds et al., 1995; see Fig. 3c). Most of the faults are small, with displacements $\leq$10 m and surface trace lengths typically $\leq$1 km, with terminations mapped in tuff. Another example of localized development of northwest-trending faults is a swarm of faults that cross West Ridge connecting the Northern Windy Wash fault and the Fatigue Wash fault (Fig. 3b and c).

In terms of the model, the western Yucca Mountain fault system presents examples of segment linkage both by lateral fault propagation of curved fault-tips (Iron Ridge and Solitario Canyon fault intersection) and by connecting fault formation (West Ridge). The regional stress field in the vicinity of Yucca Mountain evolved from east–west extension during the Miocene prior to 10 Ma, to west-northwest–east-southeast after 10 Ma (Zoback et al., 1981; Morris et al., 1996). Locally developed northwest-trending faults like those associated with corrugation of the southern Fish Slough fault segment were, therefore, probably produced by local stresses developed in relay ramps accommodating components of both regional extension and relay ramp extension rather than a complex evolution of the regional stress field.

3.3. Pleasant Valley earthquake rupture (Nevada)

The 1915 (M_s 7.6) Pleasant Valley earthquake produced discontinuous surface rupture extending 60 km along strike. The rupture was composed of four principal rupture segments (Fig. 4; see Wallace, 1984 and dePolo et al., 1991 for additional detail). These principal surface rupture segments form a right-stepping en échelon array along west-facing range fronts and are named (from south to north) the Sou Hills, Pearce, Tobin, and China Mountain segments (Wallace, 1984; dePolo et al., 1991). Surface displacement was dominantly dip-slip, and maximum vertical displacement was 5.8 m (on the Pearce segment). These ruptures were interpreted as slip on a single fault at depth (Wallace, 1984). Recently derived empirical earthquake scaling relationships (with respect to rupture area or surface rupture length; Wells and Coppersmith, 1994) predict that a single large-area rupture at depth (corresponding to the 60 km composite rupture length at the surface) would be required to produce the M_s 7.6 1915 Pleasant Valley earthquake. Slip on separate smaller en échelon faults at depth could not produce a single earthquake of such large magnitude.

Based on the lack of a surface connection of segments of the Pleasant Valley fault system, it is evident that the fault system has not yet broken through along its footwall trace. The en échelon fault segments are still separated by relay ramps. Downthrown (hanging wall) fault traces are masked by surficial deposits. The fact that the ruptures produced by the 1915 Pleasant

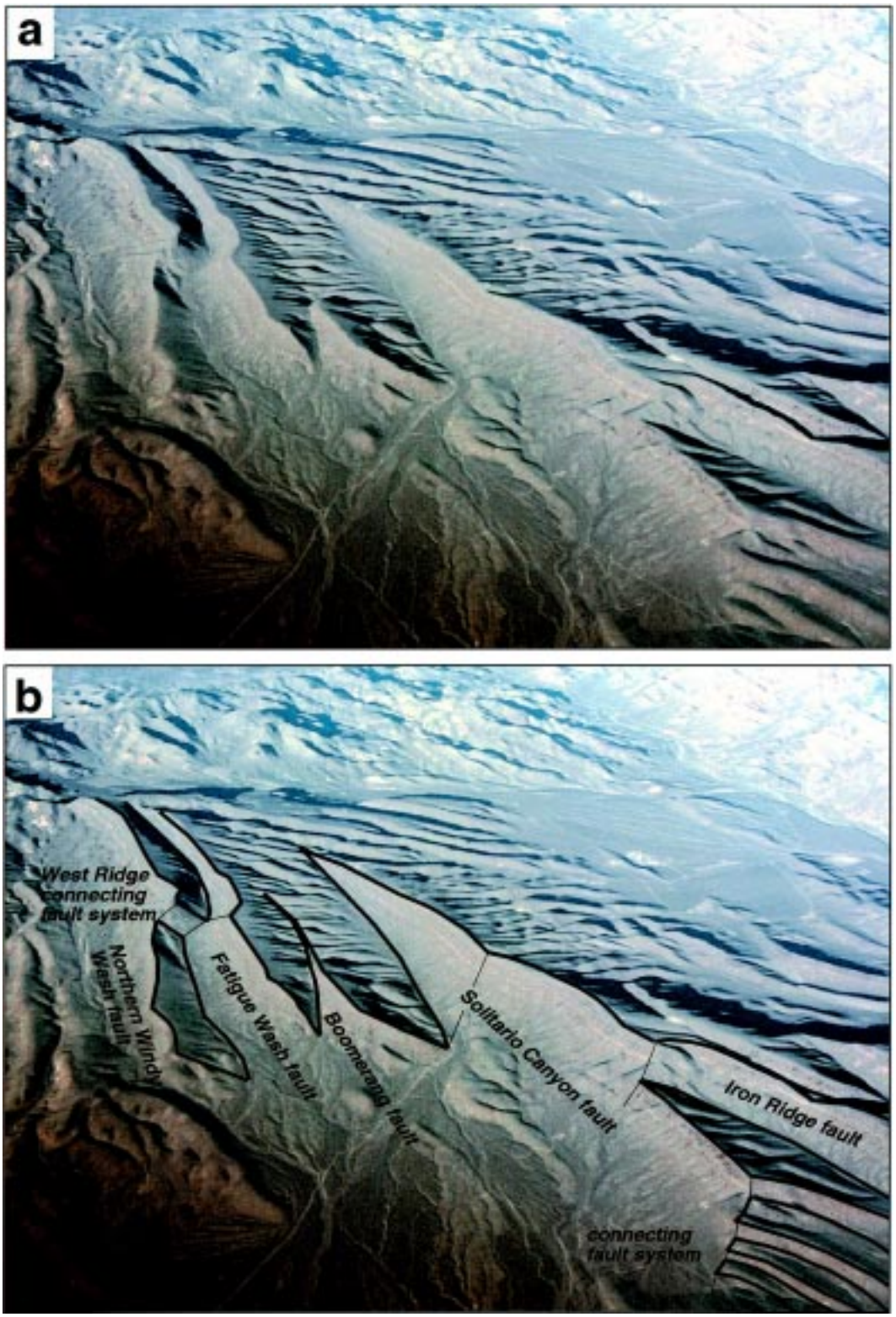

Fig. 3. An en échelon normal fault system bounds the western side of Yucca Mountain. (a) Unannotated, and (b) annotated aerial photographs (looking northeast) of Yucca Mountain, Nevada, illustrate the Solitario Canyon–Iron Ridge fault system and the overall en échelon geometry of the western Yucca Mountain fault system. (c) Map of western Yucca Mountain fault system (after Simonds et al., 1995) illustrates arrangement and connection of major faults (bold lines).

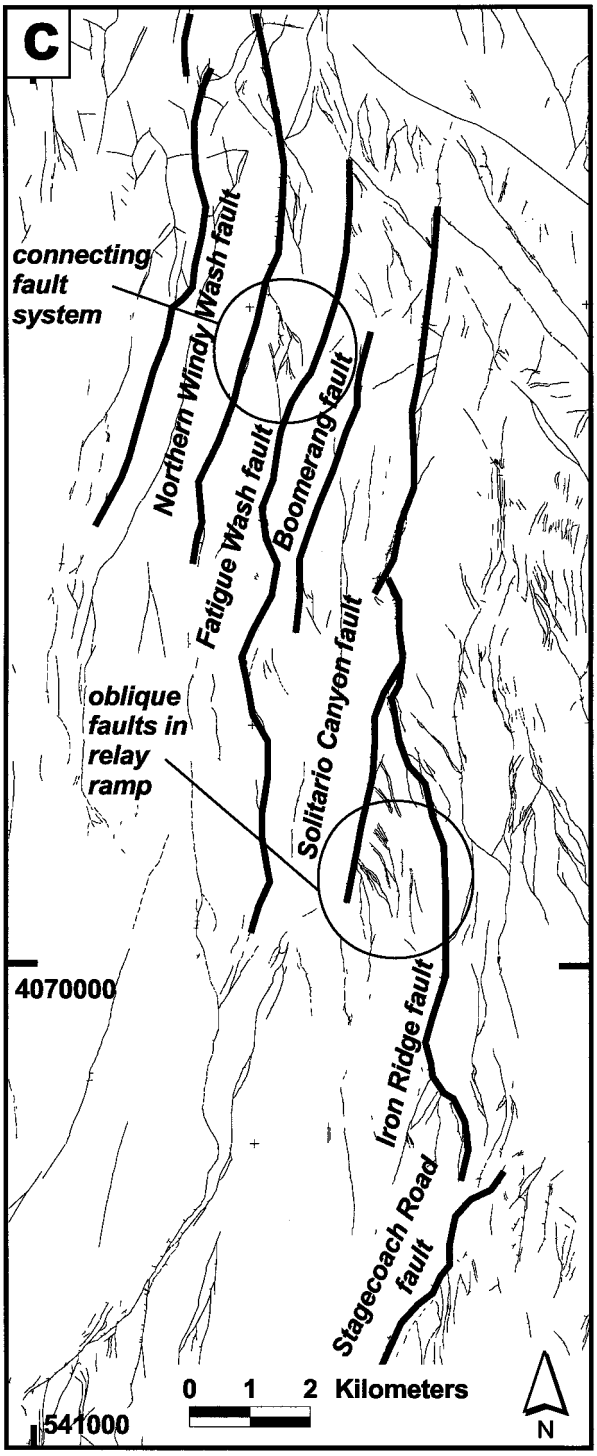

Fig. 3. (*continued*)

Valley earthquake are unconnected and overlap suggests that surface connections have not formed either along the downthrown traces or through relay ramps, at least not to the point that displacement is directly transferred from one fault segment to another. Based on these arguments, we conclude that the Pleasant Valley fault system represents an active en échelon branching normal fault with a single fault plane at depth that branches in an en échelon arrangement toward the surface (Fig. 1a, second block-diagram; also cf. Anders and Schlische, 1994). Both the north and south tips of the Pearce segment, how-

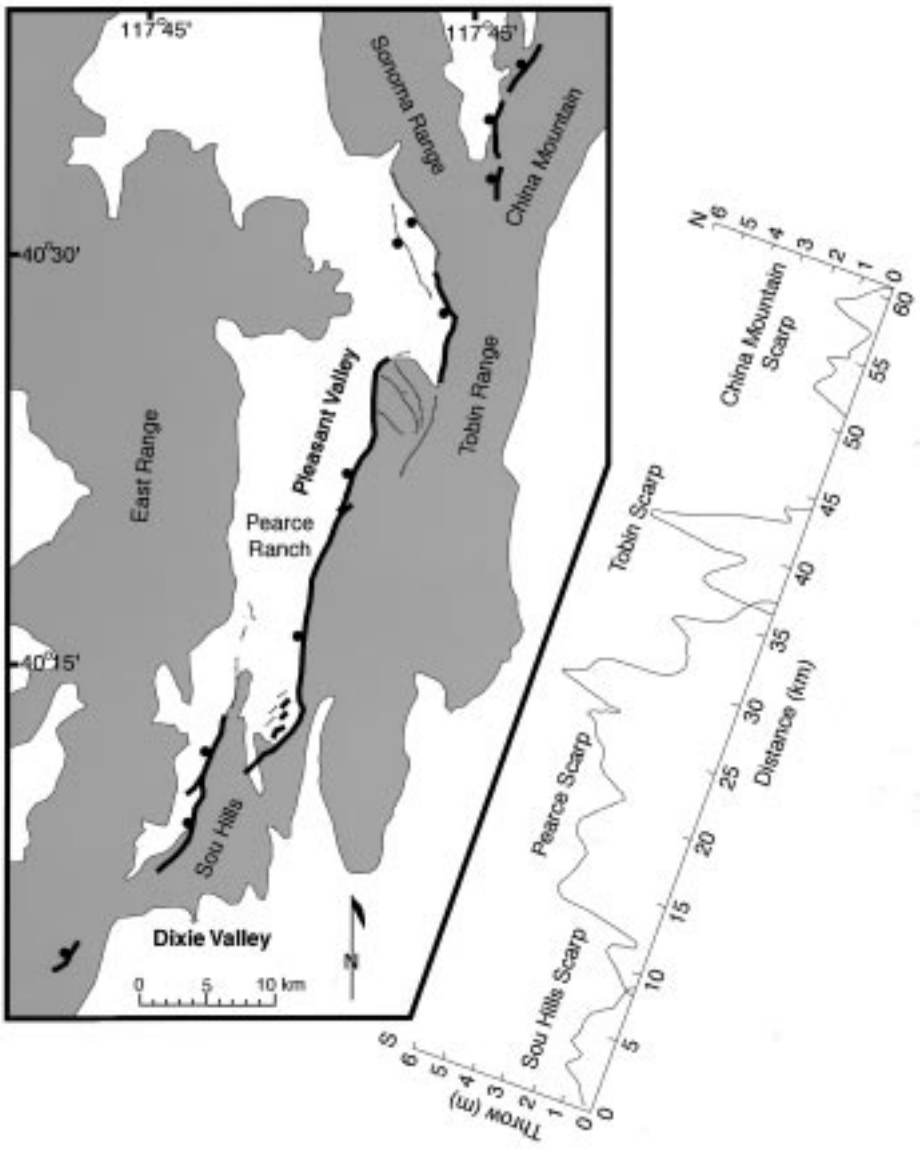

Fig. 4. Map of 1915 Pleasant Valley earthquake rupture (after dePolo et al., 1991 and Wallace, 1984) and graph of throw vs position along fault system for surface ruptures (after Wallace, 1984). Solid lines on map represent 1915 rupture, and thin dotted lines represent pre-1915 scarps and fault traces related to Pleasant Valley fault system.

ever, curve towards the adjacent overlapping fault segments, similar to the Iron Ridge fault of the western Yucca Mountain fault system. This sigmoidal fault trace shape suggests that future ruptures may ultimately lead to fault growth in which curved tips of the en échelon segments link.

In a similar fashion, the en échelon arrangement of fault offsets in the western Yucca Mountain fault system and corrugated geometry of the connected Solitario Canyon and Iron Ridge faults suggest that these faults are also part of an en échelon array or en échelon branching fault system. By analogy with the Pleasant Valley earthquake, adjacent overlapping en échelon fault segments such as the Stagecoach Road fault in the south and the Fatigue Wash and Windy Wash faults and several additional faults to the northwest may be linked at depth with the Solitario Canyon–Iron Ridge system to form a single throughgoing rupture at depth. Therefore, seismic hazard assessments for Yucca Mountain should consider the likely possibility that the en échelon faults observed at the surface are part of a large en échelon branching fault. For example, treated as individual faults, the Solitario Canyon and Iron Ridge faults yield maximum magnitude earthquakes of M_w 6.6 and 6.2, respectively. If treated as a single en échelon branching fault, then the western Yucca Mountain fault system is capable of generating earthquakes as large as M_w 6.9.

The Pleasant Valley earthquake stands as an important lesson that recognition of linked en échelon fault systems in early stages of development is critical in seismic hazard assessment.

Acknowledgements

This paper was prepared as a result of work performed at the Center for Nuclear Waste Regulatory Analyses (CNWRA) for the U.S. Nuclear Regulatory Commission (NRC) under contract number NRC-02-97-009. This paper is an independent product of the CNWRA and does not necessarily reflect the views or regulatory position of the NRC. We thank Ron Martin, Mike Conway, and Shannon Colton for their assistance in preparing data and images for this paper, Annette Mandujano for assistance in preparing the manuscript, and Larry McKague, Wes Patrick, Alan Morris, Tom Blenkinsop, and Mark Anders for technical reviews that considerably improved the manuscript.

References

An, L.-J., Sammis, C.G., 1996. Development of strike-slip faults: shear experiments in granular materials and clay using a new technique. Journal of Structural Geology 18, 1061–1077.

Anders, M.H., Schlische, R.W., 1994. Overlapping faults, intrabasin highs and the growth of normal faults. Journal of Geology 102, 165–180.

Bateman, P.C., 1965. Geology and tungsten mineralization of the Bishop District, California. USA. Geological Survey Professional Paper 470.

Bellier, O., Zoback, M.L., 1995. Recent state of stress change in the Walker Lane zone, western Basin and Range province, United States. Tectonics 14, 564–593.

Childs, C., Watterson, J., Walsh, J.J., 1995. Fault overlap zones within developing normal fault systems. Journal of the Geological Society, London 152, 535–549.

Dawers, N.H., Anders, M.H., 1995. Displacement–length scaling and fault linkage. Journal of Structural Geology 17, 607–614.

Dawers, N.H., Anders, M.H., Scholz, C.H., 1993. Growth of normal faults: Displacement–length scaling. Geology 21, 1107–1110.

Day, W.C., Dickerson, R.P., Potter, C.J., Sweetkind, D.S., San Juan, C.A., Drake, R.M., II, Fridrich, C.J., 1998. Bedrock geologic map of the Yucca Mountain area, Nye County, Nevada. U.S. Geological Survey Geologic Investigations Series, Map I-2627. Scale 1:24,000.

dePolo, C.M., Clark, D.G., Slemmons, D.B., Ramelli, A.R., 1991. Historical surface faulting in the Basin and Range Province, western North America: implications for fault segmentation. Journal of Structural Geology 13, 123–136.

Donath, F.A., 1962. Analysis of Basin–Range structure, south-central Oregon. Geological Society of America Bulletin 73, 1–16.

Ferrill, D.A., Stamatakos, J.A., Jones, S.M., Rahe, B., McKague, H.L., Martin, R.H., Morris, A.P., 1996a. Quaternary slip history of the Bare Mountain Fault (Nevada) from the morphology and distribution of alluvial fan deposits. Geology 24, 559–562.

Ferrill, D.A., Stamatakos, J.A., Morris, A.P., 1996b. Structural controls on progressive deformation of the Yucca Mountain (Nevada) region. Geological Society of America Abstracts with Programs 28, A–192.

Hancock, P.L., Barka, A.A., 1987. Kinematic indicators on active normal faults in western Turkey. Journal of Structural Geology 9, 573–584.

Holm, D.K., Fleck, R.J., Lux, D.R., 1994. The Death Valley Turtlebacks reinterpreted as Miocene–Pliocene folds of a major detachment surface. Journal of Geology 102, 718–727.

Izett, G.A., Obradovich, J.D., Mehnert, H.H., 1988. The Bishop ash bed (middle Pleistocene) and some older (Pliocene and Pleistocene) chemically and mineralogically similar ash beds in California, Nevada, and Utah. United States Geological Survey Bulletin 1675.

Lowell, J.D., 1985. Structural styles in petroleum exploration. Oil and Gas Consultants International, Inc, Tulsa.

Machette, M.N., Personius, S.F., Nelson, A.R., Schwartz, D.P., Lund, W.R., 1991. The Wasatch fault zone, Utah—segmentation and history of Holocene earthquakes. Journal of Structural Geology 13, 137–150.

Morley, C.K., 1995. Developments in the structural geology of rifts over the last decade and their impact on hydrocarbon exploration. In: Lambiase, J.J. (Ed.), Hydrocarbon Habitat in Rift Basins. Geological Society Special Publication 80, pp. 1–32.

Morris, A.P., Ferrill, D.A., Henderson, D.B., 1996. Slip tendency analysis and fault reactivation. Geology 24, 275–278.

Peacock, D.C.P., Sanderson, D.J., 1991. Displacements, segment linkage, and relay ramps in normal fault zones. Journal of Structural Geology 13, 721–733.

Peacock, D.C.P., Sanderson, D.J., 1994. Geometry and development of relay ramps in normal fault systems. American Association of Petroleum Geologists Bulletin 78, 147–165.

Platt, N.H., 1995. Structure and tectonics of the northern North Sea: New insights from deep penetration regional seismic data. In: Lambiase, J.J. (Ed.), Hydrocarbon Habitat in Rift Basins. Geological Society Special Publication 80, pp. 103–113.

Ramsay, J.G., Huber, M., 1987. The Techniques of Modern Structural Geology, Volume 2: Folds and Fractures. Academic Press, London.

Sawyer, D., Fleck, R.J., Lanphere, M.A., Warren, R.G., Broxton, D.E., Hudson, M., 1994. Episodic caldera volcanism in the Miocene southwestern Nevada volcanic field: Revised stratigraphic framework, $^{40}Ar/^{39}Ar$ geochronology and implications for magmatism and extension. Geological Society of America Bulletin 106, 1304–1318.

Schlische, R.W., Anders, M.H., 1996. Stratigraphic effects and tectonic implications of the growth of normal faults and extensional basins. Geological Society of America Special Paper 303, 183–203.

Scholz, C.H., Dawers, N.H., Yu, J.-Z., Anders, M.H., 1993. Fault growth and fault scaling laws: Preliminary results. Journal of Geophysical Research 98, 21951–21961.

Scott, R.B., 1990. Tectonic setting of Yucca Mountain, southwest Nevada. In: Wernicke, B.P. (Ed.), Basin and Range Extensional Tectonics Near the Latitude of Las Vegas, Nevada: Boulder, Colorado. Geological Society of America Memoir 176, pp. 251–282.

Simonds, W.F., Whitney, J.W., Fox, K., Ramelli, A., Yount, J.C., Carr, C.D., Menges, R., Dickerson, R., Scott, R.B., 1995. Map of fault activity of the Yucca Mountain area, Nye County, Nevada. U.S. Geological Survey Miscellaneous Investigations Series, Map I-2520. Scale 1:24,000.

Sylvester, A.G., 1988. Strike-slip faults. Geological Society of America Bulletin 100, 1666–1703.

Trudgill, B., Cartwright, J., 1994. Relay-ramp forms and normal-fault linkages, Canyonlands National Park, Utah. Geological Society of America Bulletin 106, 1143–1157.

Wallace, R.E., 1984. Faulting related to the 1915 earthquakes in

Pleasant Valley, Nevada. United States Geological Survey Professional Paper 1274-A.

Wells, D.L., Coppersmith, K.J., 1994. New empirical relationships among magnitude, rupture length, rupture width, rupture area, and surface displacement. Seismological Society of America Bulletin 84, 974–1002.

Willemse, E.J.M., 1997. Segmented normal faults: Correspondence between three-dimensional mechanical models and field data. Journal of Geophysical Research 102, 675–692.

Willemse, E.J.M., Pollard, D.D., Aydin, A., 1996. Three-dimensional analyses of slip distributions on normal fault arrays with consequences for fault scaling. Journal of Structural Geology 18, 295–309.

Zoback, M.L., Anderson, R.E., Thompson, G.A., 1981. Cainozoic evolution of the state of stress and style of tectonism of the Basin and Range province of the western United States. Philosophical Transactions of the Royal Society of London A300, 407–434.